GFZ
Helmholtz-Zentrum
POTSDAM

Originally published as:

Cesca, S., Sen, A. T., Dahm, T. (2014): Seismicity monitoring by cluster analysis of moment tensors. - Geophysical Journal International, 196, 3, pp. 1813—1826.

DOI: http://doi.org/10.1093/gji/ggt492

Geophysical Journal International

Geophys. J. Int. (2014) **196,** 1813–1826
Advance Access publication 2013 December 30

doi: 10.1093/gji/ggt492

Seismicity monitoring by cluster analysis of moment tensors

Simone Cesca,[1,2] Ali Tolga Şen[2] and Torsten Dahm[1,2]

[1] *GFZ German Research Centre for Geosciences, Telegrafenberg, D-*14473 *Potsdam, Germany. E-mail: simone.cesca@gfz-potsdam.de*
[2] *Institute of Earth and Environmental Sciences, University of Potsdam, Potsdam, Germany*

Accepted 2013 December 4. Received 2013 December 2; in original form 2013 May 14

SUMMARY

We suggest a new clustering approach to classify focal mechanisms from large moment tensor catalogues, with the purpose of automatically identify families of earthquakes with similar source geometry, recognize the orientation of most active faults, and detect temporal variations of the rupture processes. The approach differs in comparison to waveform similarity methods since clusters are detected even if they occur in large spatial distances. This approach is particularly helpful to analyse large moment tensor catalogues, as in microseismicity applications, where a manual analysis and classification is not feasible. A flexible algorithm is here proposed: it can handle different metrics, norms, and focal mechanism representations. In particular, the method can handle full moment tensor or constrained source model catalogues, for which different metrics are suggested. The method can account for variable uncertainties of different moment tensor components. We verify the method with synthetic catalogues. An application to real data from mining induced seismicity illustrates possible applications of the method and demonstrate the cluster detection and event classification performance with different moment tensor catalogues. Results proof that main earthquake source types occur on spatially separated faults, and that temporal changes in the number and characterization of focal mechanism clusters are detected. We suggest that moment tensor clustering can help assessing time dependent hazard in mines.

Key words: Persistence; memory; correlations; clustering; Earthquake source observations.

INTRODUCTION

Moment tensors are the most common and general representation of seismic sources, under the assumption of a point source approximation. A moment tensor is mathematically represented by a second-rank symmetric tensor, which is fully described by its six independent components (e.g. Aki & Richards 1980). Additional source constraints are often assumed, which reduces the number of independent variables. Source volume changes for natural earthquake source are generally considered negligible, and the isotropic source term neglected; isotropic source components are typically considered only for certain applications, for example in volcanic (e.g. Panza *et al*. 1993; Kaneshima *et al.* 1996; Legrand *et al.* 2000; Saraò *et al*. 2001; Chouet *et al.* 2003; Cesca *et al.* 2007, 2008; Lokmer *et al.* 2007; Cesca & Dahm 2008, Davi *et al.* 2010), geothermal (Panza *et al*. 1993; Kravanja *et al*. 1999; Ross *et al*. 1999; Panza & Saraò 2000; Boyd *et al*. 2011) or mining (Feignier & Young 1992; McGarr 1992a,b; Foulger & Julian 1993; Trifu *et al*. 2000; Fletcher & McGarr 2005; Julià *et al*. 2009; Vavryčuk & Kühn 2012; Cesca *et al*. 2013; Kühn & Vavryčuk 2013; Şen *et al*. 2013) environments, where changes in volume at the source may take place in consequence of multiphase processes, explosions and collapses. Volumetric source changes have been also considered for deep focus earthquake (Kuge & Kawakatsu 1990, 1992, 1993; Frolich 1995; Buforn *et al.* 2011). The isotropic component is uniquely derived from the moment tensor, through its decomposition into isotropic and deviatoric terms (e.g. Jost & Hermann 1989), and the deviatoric part further decomposed. The most widely adopted (Julian *et al*. 1998) is by far the superposition of a double couple (DC) source and a compensated linear vector dipole (CLVD) according to Knopoff & Randall (1970). A further assumption of negligible CLVD brings to the description of the source by a pure double couple, a model often used to represent the radiation pattern of a shear failure at the earthquake focus. A DC point source is generally described by means of the scalar moment and the fault plane angles (strike, dip, and rake), rather than by constrained moment tensor components.

In the last decades several codes have been proposed to invert the earthquake moment tensor. Early applications to large earthquakes at teleseismic distances leading, for example, to the Global CMT catalogue (Dziewonski *et al.* 1981; Ekström *et al.* 2012) have been later extended or adapted for the analysis of regional seismicity (e.g. Giardini *et al.* 1993, Ritsema & Lay 1993, Pondrelli *et al.* 2002, Stich *et al.* 2003, Bernardi *et al.* 2004) and weak seismicity at local distances (e.g. Şen *et al*. 2013). As a result, moment tensor catalogues are routinely generated for the whole earth and for specific regions. Moment tensor inversion, with different source constraints, is carried out by minimizing residuals between

© The Authors 2013. Published by Oxford University Press on behalf of The Royal Astronomical Society.

observations and synthetics, with the observation being either first onset polarities, body waves amplitudes, amplitude ratios, full waveforms or amplitude spectra. Possibly, the most common approach is to invert low frequency full waveform in the time domain to retrieve a deviatoric moment tensor. Polarity based approach, as well as studies to analyse the geometry of fault systems, are often carried out using a DC source representation. Finally, for specific applications (e.g. in volcanic, geothermal and mining environments), full moment tensors are inverted.

If the analysis of focal mechanisms for single events or a limited number of earthquakes can be easily evaluated to discuss the fault geometry or to invert for local stresses, the automated analysis of large moment tensor catalogues require the setup of specific tools. These should be able to automatically recognize the most dominant source characteristics of the target seismicity, identify families of events with similar focal mechanisms, and share the earthquake catalogue according to the chosen classification. We propose here to use clustering techniques to this purpose. Data clustering is the task of assigning a set of objects into clusters, which are group of objects similar among them. Event clusters are not predefined, but automatically detected through the cluster analysis. A broad range of clustering techniques have been proposed in the past, and applied to a very broad range of scientific fields; a wide literature describes different techniques and corresponding algorithms. In this paper we limit the discussion to the use of a density-based clustering algorithm, namely DBSCAN, and combine it with the definition of different metrics, which can be used to define the distance among source models, according to different moment tensor representations. Clustering approaches have been used in seismology so far mostly to recognize events patterns and identify foreshocks and aftershocks based on the spatial location (Ouillon & Sornette 2011; Konstantaras *et al.* 2012; Lippiello *et al.* 2012), temporal evolution (Kagan & Knopoff 1976; Kagan & Jackson 1991, Hainzl *et al.* 2000) or on the analysis of spatiotemporal distribution of seismicity (Hainzl *et al*. 2000; Sornette & Werner 2005). Waveforms similarity has also been used for clustering approaches (Maurer & Deichmann 1995; Cattaneo *et al.* 1999; Wehling-Benatelli *et al.* 2013); however, since similar waveforms are observed when both the source radiation patterns (i.e. the focal mechanism) and the source locations are similar, the approach and expected classification results are different to those here discussed. Finally, focal mechanism clustering have been proposed by Willemann (1993), which tested hierarchical clustering techniques to classify focal mechanisms using a moment tensor representation. Following the developments of moment tensor inversion techniques and new clustering techniques in the last decades, we extend the former approach by Willemann (1993) through the adoption of DBSCAN clustering, the comparison of different metrics for different source representations, and the discussion of moment tensor inversion uncertainties within the clustering framework. Moreover, we discuss the application of moment tensor clustering to monitor the temporal evolution of seismicity, in order to detect the appearance of anomalous rupture processes improving seismic hazard assessment. This is extremely important, for example, in mining, geothermal, gas/oil and water reservoirs exploitation environments, where different geoengineering operations can strongly modify the characteristics of fracturing processes.

METHODOLOGY, CLUSTERING METHOD

Clustering techniques are devoted to the automated classification of object into classes, or clusters, characterized by similar objects. Any clustering technique requires the definition of a metric, to be used to evaluate the similarity (or dissimilarity) among the objects within the studied data set. Several techniques have been proposed in the last decades. They may lead to different clustering results depending on adopted algorithms and parametrizations. We adopt here a density-based clustering approach, DBSCAN (Ester *et al.* 1996). DBSCAN, as a density-based clustering technique, is based on the observation that data clusters are characterized by a high density of points (in this case, moment tensors), much higher than outside of the cluster, and that outliers are sparsely distributed, in regions of much lower density than for any cluster. Such an approach will identify a cluster as a densely populated region, with no constraints on its shape. The inclusion of a point in a cluster with DBSCAN is based on the concept of density reachability, which is here briefly recalled (for more details, see Ester *et al.* 1996). It is likely that the cluster will be more densely populated in its inner part and less populated at the edge. From this consideration, DBSCAN defines core points those ones located in a dense region: formally, a core point has a sufficient number of points ($N_{\min}$) in its neighbourhood (which is defined on the base of a threshold distance, ϵ). Points located in the neighbourhood of the core point are defined as directly reachable from the core point. If such target points are still located in a dense region, they are also identified as core points of the cluster. Otherwise, when they are in a more sparse region, they are defined as border point and will result at the edge of the cluster. The neighbourhood of a border point is much less populated than the one of a core point, nevertheless the border point still pertains to a cluster, because it is directly reachable from a core point. Following the DBSCAN formalism, all points of a cluster are then said density-reachable, and the cluster densely connected. Core point can be identified by checking the populations in their neighbourhood. Each of them can create a cluster, together with the points in their neighbourhood. Connected clusters will be merged into single clusters. Points with sparsely populated neighbourhood and which are not densely reachable by any core point will be identified as noise. The performance of DBSCAN is entirely controlled by two parameters: the threshold value ϵ, which defines the maximal distance at which a target event is considered directly reachable from a core point, and $N_{\min}$, which is a measure of the density of a given region, defined as the minimum number of the points which have to be situated within the distance range. $N_{\min}$ is also a constraint for the minimal size of a cluster. DBSCAN has several qualities, which make it appealing for the aim of clustering focal mechanisms and moment tensor solutions. First of all, the algorithm has the concept of noise, so that not all events have to be part of a cluster. This feature is important to treat outliers, which are likely present in a moment tensor catalogue, but may not be easily identified for large catalogues. A second, relevant features is its stability against the sorting of the input catalogues, whereas other methods may provide different clustering results depending on the way the original catalogue is sorted. This feature make the clustering result unique, at least with respect to the catalogue sorting. Finally, DBSCAN does not require a predefined number of clusters, a feature which is anyhow common to many other algorithms. As a drawback, DBSCAN may be unable to separate close clusters, unless through a precise tuning of its parameters, ϵ and $N_{\min}$. Moreover, the choice of these parameters is somehow subjective and can affect the number, size and heterogeneity of identified clusters. The problem is further discussed in the following section on synthetic tests. Previous attempts to cluster moment tensor solutions (Willemann 1993) only made use of hierarchical clustering techniques; density-based techniques such DBSCAN have never been used before to this purpose.

The DBSCAN technique has been implemented within our software, making use of a suitable python library within scikit-learn (Pedregosa *et al.* 2011).

METHODOLOGY, DISTANCE BETWEEN MOMENT TENSORS

Different distances among moment tensors have been proposed in previous studies (Kagan 1991, 1992; Willemann 1993; Tape & Tape 2012) and will be here discussed and further extended. The Kagan angle approach (Kagan 1991, 1992) aims to describe the difference among pure DC source models. It has the beauty to be intuitive, as it is based on the transformation of a DC focal mechanism into a second one through rotations. Using the quaternion convention, a single rotation is sufficient and the rotation angle (later referred as Kagan angle) can be used as a measure of this distance. In order to have a distance d ranging [0,1], the rotation angle is here divided by 120°, which is the maximal possible Kagan angle among two DC focal mechanisms (note that in the following plots, a similarity coefficient is defined as 1–*d*, so that the value 1 is assigned in case of maximal similarity):

$$d = \xi_0/(2\pi/3), \tag{1}$$

where ξ_0 is the Kagan angle (see Kagan 1992 for details on its computation).

The other considered metrics are more general and based on a moment tensor representation. They are thus useful to compare full and deviatoric moment tensor mechanisms, but can also be used for pure DC cases. Willemann (1993) proposed to use coherence, where similarity is assessed on the base of the cosine angle among vectors composed by moment tensor components. A cosine-based approach was also proposed in Tape & Tape (2012), where the formalism is more suited to build a distance definition which ranges between 0 and 1. Upon eq. (67) in Tape & Tape (2012), we can define the distance among two moment tensors M and N (with elements m_{ij} and n_{ij}, respectively) as:

$$d = \frac{1}{2}\left[1 - \frac{M \cdot N}{\|M\|\,\|N\|}\right] = \frac{1}{2}\left[1 - \frac{\sum m_{ij} n_{ij}}{\left(\sum m_{ij}^2\right)^{1/2}\left(\sum n_{ij}^2\right)^{1/2}}\right] \tag{2}$$

with summation over both indices. The distance is computed using the standard inner product in IR^9. Considering that moment tensor are characterized by six independent moment tensor components, which are the typical output of moment tensor inversions, the following modification of the previous distance could be considered:

$$d = \frac{1}{2}\left[1 - \frac{\sum m_i n_i}{\left(\sum m_i^2\right)^{1/2}\left(\sum n_i^2\right)^{1/2}}\right], \tag{3}$$

where m_i and n_i are the independent components of moment tensors and the inner product is performed in IR^6. Other possible metrics, treating the independent moment tensor components as vectors could make use of normalized L^1 and L^2 norms.

Fig. 1 illustrates the distance increase with respect to a reference DC model (normal faulting, strike 0°, dip 45° and rake –90°). The first cases (Figs 1a–d) refer to DC perturbations, by increasingly change the strike, dip, rake or the three angles at a time. The Kagan angle shows some nice features: it has a linear relation with the rotation angle and the same rotation of strike, dip or rake angles lead to the same distance. The adoption of the Kagan angle for focal mechanism comparison was criticized by Willemann (1993), upon the fact that focal mechanisms with opposite polarities are not considered the most dissimilar (the Kagan angle among them is 90°, whereas the maximal Kagan angle value is 120°). However, the maximal Kagan angle is found for focal mechanisms pairs, which can be considered even more dissimilar in terms of rupture geometries: for example, certain pairs of normal and thrust mechanisms with perpendicular strikes.

The remaining tested distances (see Fig. 1) do not accomplish the previous properties of the Kagan angle distance. The only exception is the cosine distance in R^9, which shows a linear behaviour with the rotation angle, but still differ for common variations of strike, dip and rake angles. However, these distances remain useful, at least, for the case of full and deviatoric moment tensors, where the Kagan angle cannot be used. Figs 1(e)–(f) illustrates this case, showing how the L^1, L^2 and cosine distance perform, when the original focal mechanism is perturbed through the inclusion of increasing CLVD (Fig. 1e) and isotropic (Fig. 1f) components. Note that maximal perturbed cases correspond to pure CLVD and ISO sources. Cosine distance in R^9 and R^6 have the same performance, because off-trace components are invariant for the selected range of moment tensors.

It is worth to note that all these distance makes no use of uncertainties of the moment tensors solutions. Moment tensors are typically the results of specific inversion routines, based on the fit of a part of the seismic data (e.g. polarities, amplitudes and waveforms), and relying on variable data sets and limited knowledge of wave propagation. They are significantly affected by several factors, including the source depth, the network geometry, the signal quality, the simplified adopted velocity models, and the inversion framework. As a consequence, moment tensor solutions may have relevant uncertainties: however, these are typically not comparable for all moment tensor components. For example, Henry *et al.* (2002) showed that M_{xz} and M_{yz} components are poorly resolved for shallow earthquakes using low frequency full waveforms, because their Green's functions vanish at the free surface. Bukchin *et al.* (2010) showed how this can lead to ambiguous focal mechanisms solutions. Du & Warpinski (2011) discussed the effects of moment tensor uncertainty effects on fault plane solutions for microseismicity studies. In other cases, because of the source-network geometry and the inversion approach, the distribution of uncertainties may be different. The problem is here illustrated for the coal mining induced seismicity data set, which will be analysed in the following of this work. Moment tensor components uncertainties have been here assessed using synthetic tests. We considered events with different locations (epicentres at the edges of the mined area where the seismicity is concentrated, see Grigoli *et al.* 2013) and typical focal mechanisms (normal faulting parallel to mine walls and stope, see Şen *et al.* 2013). For each reference mechanism and location, we estimated the misfit increments, when perturbing separately each single MT component of the original focal mechanisms by 20 per cent; misfits were computed among amplitude spectra using an L^2 norm, reproducing the exact inversion conditions as for the derivation of the MT catalogue. A small misfit among the true and perturbed mechanism indicates a worse condition to discriminate among both source model, thus pointing to a larger uncertainty on the tested MT component. Results are illustrated in Fig. 2: although results slightly change when considering variable locations and reference mechanisms, these variations are minor, compared to those among MT components. In particular, horizontal dipoles M_{xx} and M_{yy} are the least resolved components, whereas M_{xz} and M_{yz} are the best constrained. Similar results were also found on the base of the distribution of MT results from a jack-knife analysis, considering a very limited data set composed of six selected events (Şen *et al.* 2013).

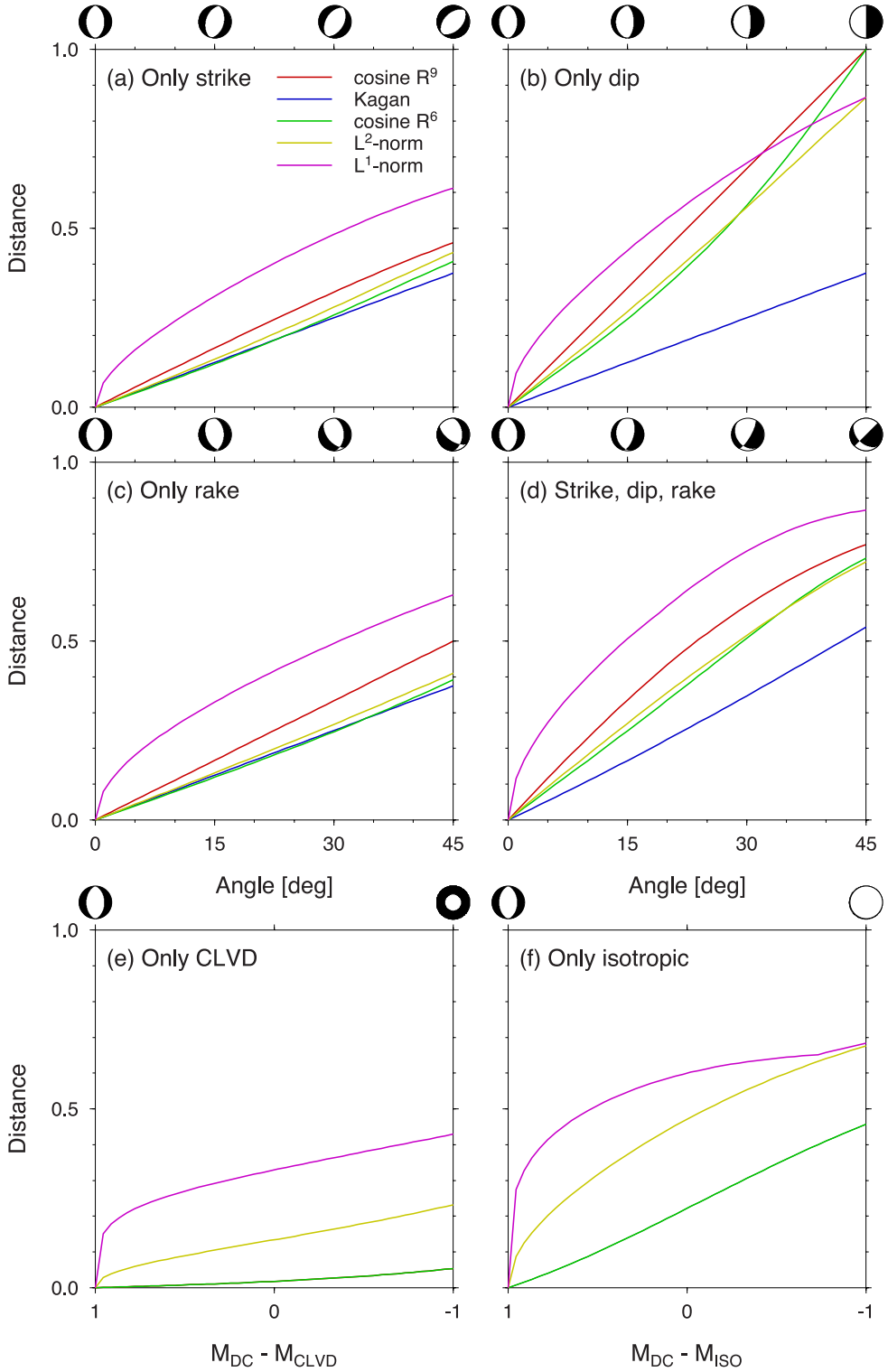

Figure 1. Performance of difference distance definitions. Distances are computed for five metrics (colours according to the legend in the top left-hand plot), among a reference pure DC focal mechanism (strike 0°, dip 45° and rake –90°) and perturbed mechanisms. DC focal mechanisms perturbations (top) are obtained by rotating progressively (see focal spheres) the reference mechanisms up to 45° of strike (a), dip (b), rake (c) and all three (d) angles. Perturbed mechanisms including non-DC components are shown in the bottom plots for four metrics (the Kagan angle is not applied as it cannot handle). Mechanism perturbation is performed by adding increasing CLVD (e) and ISO (f) components, in a way that moment tensor remain normalized; most perturb cases correspond to pure CLVD and ISO mechanisms.

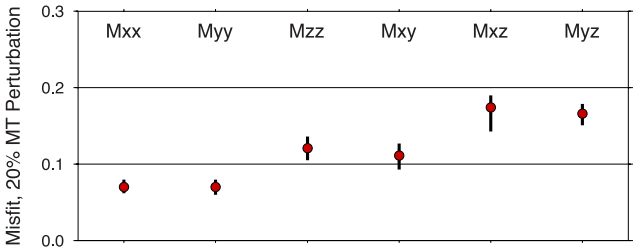

Figure 2. Mean values (red circles) and range of values (black bars) of misfits obtained when comparing original amplitude spectra and synthetics for perturbed moment tensors, following the inversion approach used by Şen *et al*. (2013). The figure illustrates the overall result of repeated tests, considering different locations and focal mechanisms. Smaller misfits, corresponding to larger MT component uncertainties, can be used as weights for the weighted MT clustering approach.

On the base of these considerations, moment tensor components uncertainties should be accounted in the definition of the distance. Adopting the cosine-distance, we propose to use the following equation:

$$d = 1 - \frac{\sum w_i^2 m_i n_i}{\left(\sum w_i^2 m_i^2\right)^{1/2} \left(\sum w_i^2 n_i^2\right)^{1/2}}, \qquad (4)$$

where each w_i is a weighting factors for a moment tensor component i. Weighting factors can be defined, for example, as reciprocals of uncertainties. Note that distances defined according to Willemann (1993) and Tape & Tape (2012), as in eq. (2), as well as eq. (3), are specific cases of eq. (4), upon certain weights selection. A similar weighting approach can also be applied to L^1 and L^2 norm distances. It is important to remind that the proposed weighting scheme, assigning fixed weights to single MT components, should only be used if the distribution of uncertainties is similar for the whole considered data set. It is possible, in fact, that MT component uncertainties vary among events with different locations, depths, focal mechanisms or magnitudes. The weighting scheme should in any case be tested when considering seismogenic region, which are large in comparison to the network, or if strong network changes took place during the catalogue time (a temporal evolution of the network could affect MT uncertainties in different time spans). An alternative approach, when the moment tensor catalogue is dominated by moment non-DC terms, for example, in presence of tensile cracks with dominant tensional (or compressive) CLVD, a different approach could be considered, with a distance mostly based on the similarity among tension (or pressure) axis orientations, and down-weighting the poorly resolved orientation of the remaining axis.

Cluster mean parameters can be obtained for each cluster. They should be computed on the base of the distance definition adopted for the clustering. The mean parameters should ensure the minimization of the sum of the distances to cluster members. For the Kagan angle definition, the mean triple (strike, dip, rake; in the following with the notation φ, δ, λ) can be obtained by scanning the whole space of possible triples (φ, δ, λ), to find the triplet for which is minimized the summed Kagan distance over the n members of the cluster:

$$(\bar{\varphi}, \bar{\delta}, \bar{\lambda}) = \left\{ (\varphi, \delta, \lambda) : \min \sum_{i=1,n} \xi_0 \left((\varphi, \delta, \lambda), (\varphi_i, \delta_i, \lambda_i) \right) \right\}, \qquad (5)$$

where the scan of the triples can be optimized upon the distribution of strike, dip and rake of cluster members. For cosine-based definitions, included weighted ones, averaging of moment tensor components provides the searched mean values.

SYNTHETIC TESTS

Prior to the application to real data, we discuss the performance of the proposed clustering technique on a synthetic moment tensor data set. The synthetic catalogue is composed of 500 events, with the following dominant mechanisms: (1) 20 per cent are close to pure DC mechanism with normal faulting of common orientation (focal mechanism A: strike 80°, dip 45°, rake –90°), (2) 20 per cent are generated with focal mechanism A superposed to a negative tensile component (50 per cent of the energy release, the principal axis oriented vertically), (3) 20 per cent are dominated by a second, different pure DC focal mechanism associated to normal faulting of different orientation (focal mechanism B: strike 130°, dip 45°, rake –90°), (4) 20 per cent have focal mechanism B superposed to a negative tensile component (50 per cent of the energy release, the principal axis oriented vertically) and (5) the remaining 20 per cent is composed by dominant shear crack events of random faulting style. For each event, full moment tensor components are derived, normalized to a scalar moment of 1 Nm. Each moment tensor component is then randomly perturbed up to ±0.1 Nm (off-trace components) or up to ±0.2 Nm (trace components). In this way a full moment tensor catalogue is generated. A second, pure DC catalogue is obtained from the previous one, only considering the DC term, after a moment tensor decomposition (ISO+CLVD+DC, see Jost & Hermann 1989; Krieger & Heimann 2012).

We start considering the DC catalogue and apply the clustering using the Kagan angle metrics (eq. 1). Results are shown in Fig. 3(a), through similarity matrices, sorted chronologically (left-hand panel) and upon clustering (right-hand panel). The plot illustrates the correct resolution of two clusters, accounting each for 40 per cent of the catalogue, and a noise cluster, accounting for the remaining 20 per cent of the earthquake source models. The two main clusters are composed by events of type (1) and (2), and (3) and (4), respectively, because the non-DC terms cannot be resolved in this approach. The analysis of the full MT catalogue (Figs 3b and c), is performed both using a cosine distance in IR[9] (Fig. 3b), according to eq. (2), and using a weighted distance (Fig. 3c), according to eq. (4). Both approaches lead to the correct resolution of the four original clusters; the 20 per cent of random DC mechanisms of group (5) are properly identified as noise. As expected, the two clusters of combined DC+tensile crack events show some similarity to their relative pure DC clusters. For the chosen synthetic tests setup, weighted and unweighted moment tensor clustering estimate comparable similarity values (average distance of 0.15 among different pure DC clusters, 0.06 among different non DC clusters, and 0.08 among a DC cluster and its corresponding non-DC cluster, with similar orientation of the DC component). On these synthetic data set, the DBSCAN algorithm can successfully distinguish the original clusters for all discussed metrics. For both synthetic tests, the DBSCAN algorithm was tuned using $N_{\min} = 10$ and $\epsilon = 0.90$.

CLUSTERING OF MINING INDUCED SEISMICITY

To illustrate possible applications of moment tensor clustering, we consider a mining induced microseismic data set. Although the method has similar potential applications for the analysis of natural seismicity, the induced seismicity data set is here chosen because

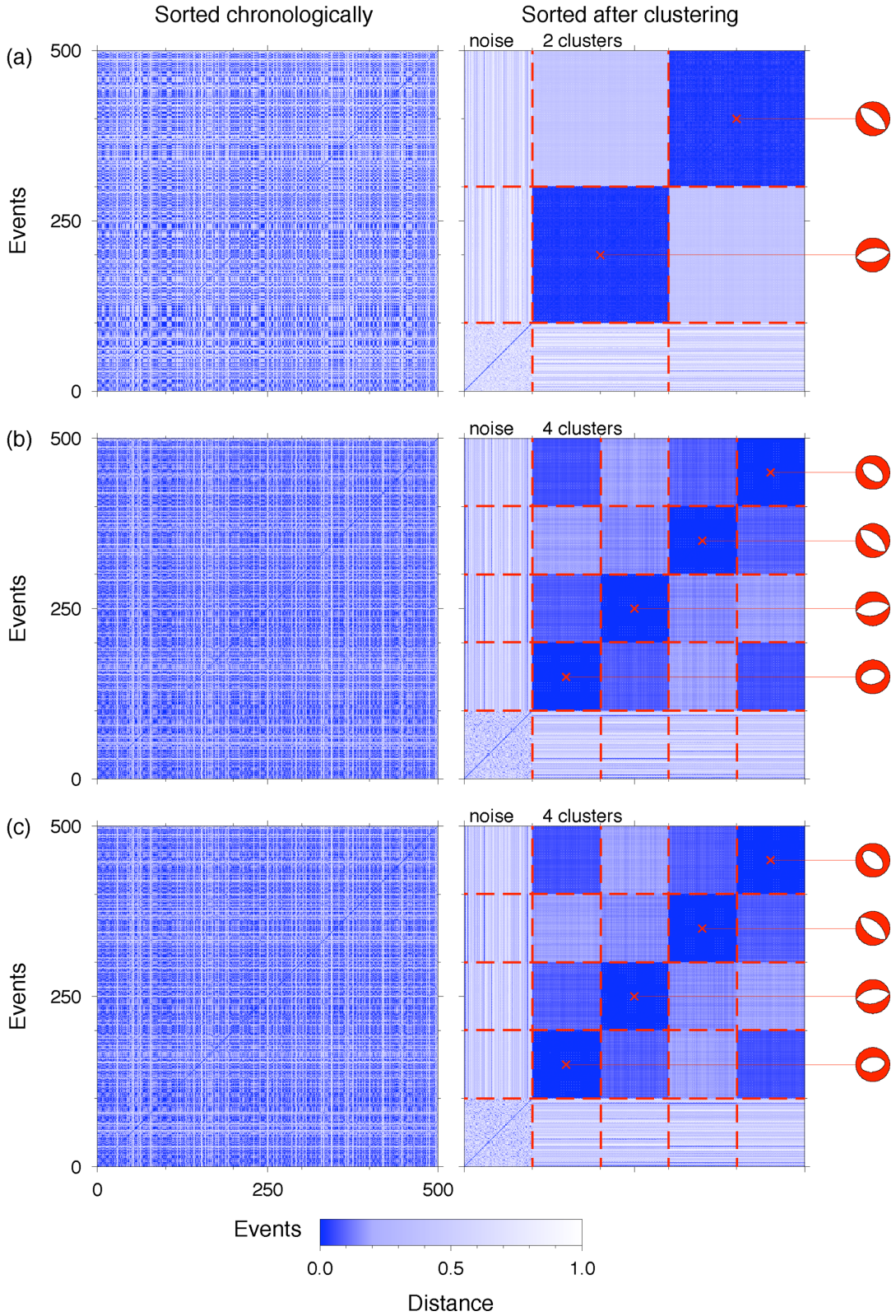

Figure 3. Synthetic test results for pure DC (a), and full MT (b, c) clustering are shown in terms of similarity matrices, according to the colour scale below. A Kagan angle distance is used for the DC approach, and both unweighted cosine distance according to eq. (2) (b) and weighted cosine distance as in eq. (4) (c) for the MT approach. Similarity matrices are plotted before clustering, sorting events chronologically (left-hand panels), and after clustering, sorting them upon their cluster (right-hand panels). Average focal mechanisms are shown on the right-hand side for each cluster, except for noise.

of the strong temporal and spatial variation of seismicity, the occurrence of different, repeatable focal mechanisms, the possible presence of non-DC, tensile and isotropic sources, and the occurrence of specific failures in correspondence to geoengineering operations. This makes it an optimal case to discuss the overall identification and characterization of source clusters, as well as the adoption of the focal mechanism clustering technique for monitoring purposes. The study region is located close to the town of Hamm, in the Ruhr region, Germany. In the Ruhr region, coal mining has been performed for centuries, and mining induced seismicity seismically monitored since 1983 (Bischoff *et al*. 2010). We focus here on induced seismicity taking place between 2006 June and 2007 July, in consequence of the long-wall mining of a rectangular-shaped panel in the region Hamm-Heringen. During almost 14 months, more than 7000 events were located, 3000 of them with magnitude above M_L –0.5. Moment tensor solutions are available for 1169 events, following the work of Şen *et al*. (2013), based on the inversion of full waveform amplitude spectra and displacement traces at surface stations located at local distances (below 2 km). The multistep inversion approach adopted by Şen *et al*. (2013) made available two moment tensor catalogues: one for pure DC and one with full MT solutions. Note that these catalogues are the result of two different amplitude spectra inversion setups; the DC catalogue is composed by the best-fitting focal mechanism solutions, assuming a pure DC constraint, and it is not simply listing the DC components of the full MT solutions. Hypocentres are spread around the average depth of 1000 m, with ruptures mostly taking place just above the mining level. According to a first, qualitative classification of focal mechanisms, almost all events are characterized by normal faulting, with a fault plane steeper than 45° and one shallower than 45°. Strike angles have a more complex distribution, but a correlation with the orientations of sides and stopes of the rectangular mined region have been suggested (Şen *et al*. 2013). Moment tensor solutions often indicate relevant non-DC components, which are interpreted as a combination of tensile crack (opening cracks occurring more often than closing cracks) and shear faulting.

We first consider the pure DC catalogue and used the Kagan angle approach to perform the source clustering. Upon checking different values for N_{min} and ϵ, DBSCAN is finally performed using $N_{min} = 10$ and $\epsilon = 0.90$ (the effect of a variation of these parameters is commented in the discussion section). Results are illustrated in Fig. 4 and show that five main clusters are identified. Their average focal mechanisms are shown in Fig. 4(c). Note that the adopted representation, showing only strike, dip and rake angles for one (steeper) fault plane, is only possible because of the favourable circumstance that many (more than 92 per cent) events have a steeper (more than 45°) and a shallower (less than 45°) dipping, which make the mechanism unambiguously describe by fault plane angles of one plane. Clusters are here sorted upon their size. Cluster 2 (303 events) and 5 (16 events) are relatively similar among them and their normal faulting focal mechanisms striking in direction NE–SW and N–S, with one plane commonly striking parallel to the panel wall (about N 60° E); the smaller Cluster 5 has a larger oblique component. Cluster 1 (360 events), 3 (119 events) and 4 (78 events) also have similar features, striking subparallel to the panel sides, which are oriented WSW–ENE; the steeper plane of clusters 1 and 4 dip towards SW, and towards NE for cluster 3. Finally, 301 events are considered as noise.

A second application to the full MT catalogue was performed using a weighted cosine distance, according to eq. (4). Weights for the six moment tensor components were chosen as it follows, based on the estimated perturbation misfits (see Fig. 2): $w_{xx} = 0.41$, $w_{yy} = 0.41$, $w_{zz} = 0.71$, $w_{xy} = 0.65$, $w_{xz} = 1.00$ and $w_{yz} = 1.00$. DBSCAN run with analogous parametrization as for the DC clustering. Results are illustrated in Fig. 5. Six clusters are found. Cluster 1 and 2 are the largest, with 357 and 141 events, respectively; Clusters 3 and 4 are similar to Cluster 2, while Clusters 5 and 6 are similar to Cluster 1. 538 focal mechanisms are not assigned to any cluster and considered as noise. Fig. 5(c) shows the source type diagram representation (Hudson *et al.* 1989). It illustrates how the two main identified clusters are characterized by full moment tensor composed by a superposition of DC and tensile components. However, Cluster 1 is characterized by a positive tensile crack component, while Cluster 2 by a negative one. Both clusters include events with variable orientation of the DC component. Only smallest clusters (e.g. Clusters 5 and 6), which are more compact, contain events with similar decomposition and similar DC mechanism. It is important to point out that MT clustering does not necessarily highlights the different moment tensor decomposition. This result is found here because of the unpopulated region at the centre of the Hudson plot, which separates regions (clusters) with denser populations of moment tensors.

TEMPORAL MONITORING OF RUPTURE PROCESSES

The previous section illustrated the identification of clusters and their characterization, through the evaluation of average focal mechanisms for each cluster. Induced seismicity data set, such as the mining data set here considered, may be characterized by a strong spatio-temporal variation, as a consequence of discontinuous geomechanical activities and their translation in space at different time and phases of the exploitation. The spatio-temporal migration of seismicity, which is well observed for the studied data set, is not relevant here. However, this can well be accompanied by changes in the brittle failures. A temporal analysis of the number and characteristics of focal mechanism clusters is thus important for monitoring purposes, in order to early detect anomalous rupture mechanisms. Limiting to mining environments, the appearance of new DC mechanisms may indicate the activation of pre-existing faults, and strong non-DC terms may indicate anomalous tensile components. Since the magnitude frequency distribution of DC and tensile events typically differs (e.g. Becker *et al.* 2010), the clustering technique can thus provide a valuable contribution towards temporal evolution of hazard assessment in the mine. The temporal evolution of different clusters, in terms of number of events, is illustrated in Fig. 6. Induced seismicity mostly takes place between day 30 (reference day 0 is 2006 July 14) and day 270. While at the beginning of the exploitation clusters 1, 3 and 4 are dominant, in the second phase, after day 150, most seismic events pertain to cluster 2. Cluster 5 is only activated at a later stage, between days 200 and 260.

We discuss here a possible approach of source clustering for monitoring purposes, with respect to the analysis of the DC catalogue for the Hamm region, simulating the temporal evolution of the catalogue. Since the moment tensor inversion is performed within 3 min and clustering of a catalogue of about 1000 events within 1 min on a single processor, the clustering application can work in near-real time. In terms of the warning time required to detect the appearance of a new cluster, these computation times may be negligible for many applications. More often, the warning time will be controlled by the seismicity rate and the N_{min} parameter. In fact, a new cluster will only be detected when a sufficient number of event with a new focal mechanism type have been identified. Before this time, they

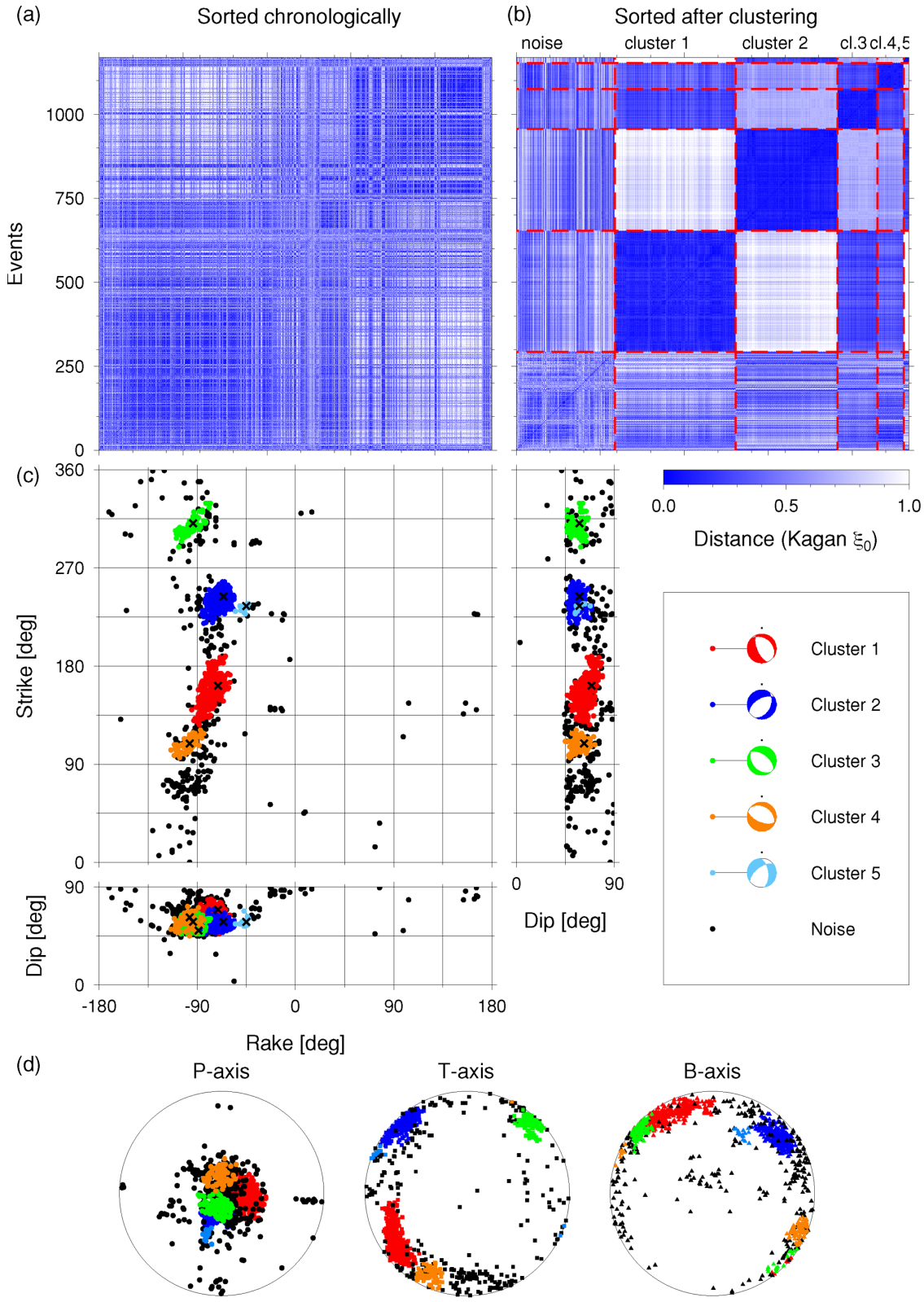

Figure 4. Results of DC clustering of a coal mining induced data set, Ruhr, Germany. Similarity matrices are shown before (a) and after (b) clustering. Red dashed lines indicate noise events and indentified clusters. Strike, dip and rake parameters are plotted (c) along strike-dip, rake-dip and strike-rake diagrams, according to the colour legend on the bottom right. Mean focal mechanisms are plotted with the same colour scale. Plots (d) illustrate the distributions of pressure (P), tension (T) and null (B) axis for different clusters (a Lambert azimuthal equal-area projection is used).

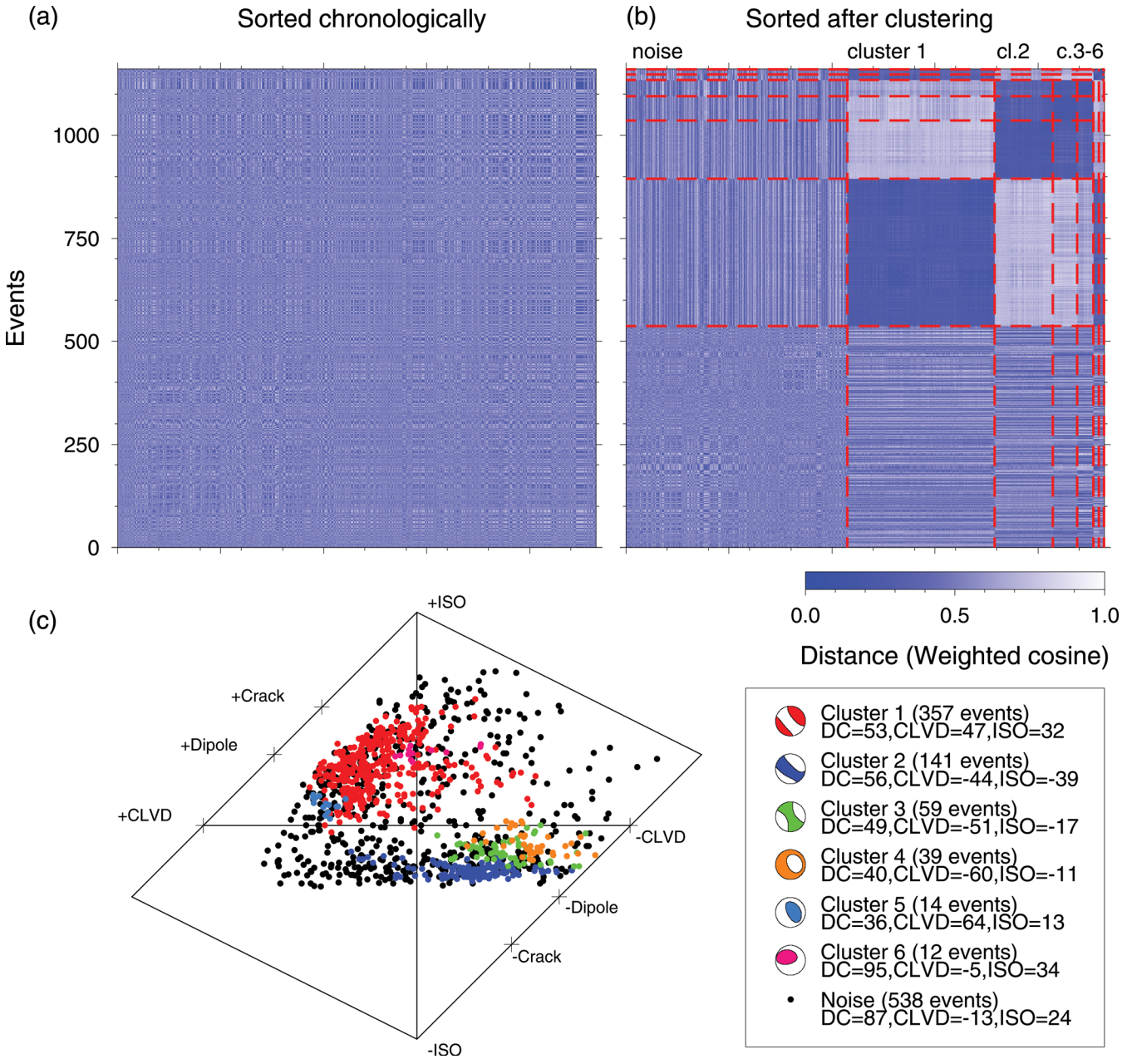

Figure 5. Results of MT clustering of a coal mining induced data set, Ruhr, Germany. Similarity matrices are shown before (a) and after (b) clustering. Red dashed lines indicate noise events and indentified clusters. Source models are plotted using a source-type diagram (c), according to the colour legend. Mean values for the MT decomposition and mean focal mechanisms are given for each cluster, except for the noise one.

are identified as noise, and might only be detected looking at the noise rate; this option is not investigated in this work. The monitoring starts here after a learning period of 30 d, which is needed to have a sufficient number of earthquakes focal mechanism solutions. The clustering analysis is routinely repeated (in the example in Fig. 7, every 10 d) considering either the whole seismic catalogue until the current date, which we refer as cumulative seismicity approach, or only the events of a previous period (here 30 d), which we refer as time window approach. The number and characteristics of the clusters are iteratively updated. A change in the cluster mean values or the appearance/disappearance of a new cluster can be used as a warning signal and trigger more detailed source analysis and an update of the hazard assessment. The cumulative seismicity approach (Fig. 7d, green line) is suited to monitor the overall seismicity: the number of events increases with time while the clustering approach becomes more stable. The time window approach (Fig. 3d, red line) may be less stable during periods of weaker activity, but it can also detect the disappearance or weakening of previously active clusters. Results are illustrated in Fig. 7, where a snapshot (at day 270) of the monitoring framework is shown. The different panels on the top of the figure illustrates the spatio-temporal distribution of the hypocentres, their spatial correlation with the mined region, and the spatial distribution of different clusters. These plot are produced using the overall catalogue until the current monitoring day (day 270).

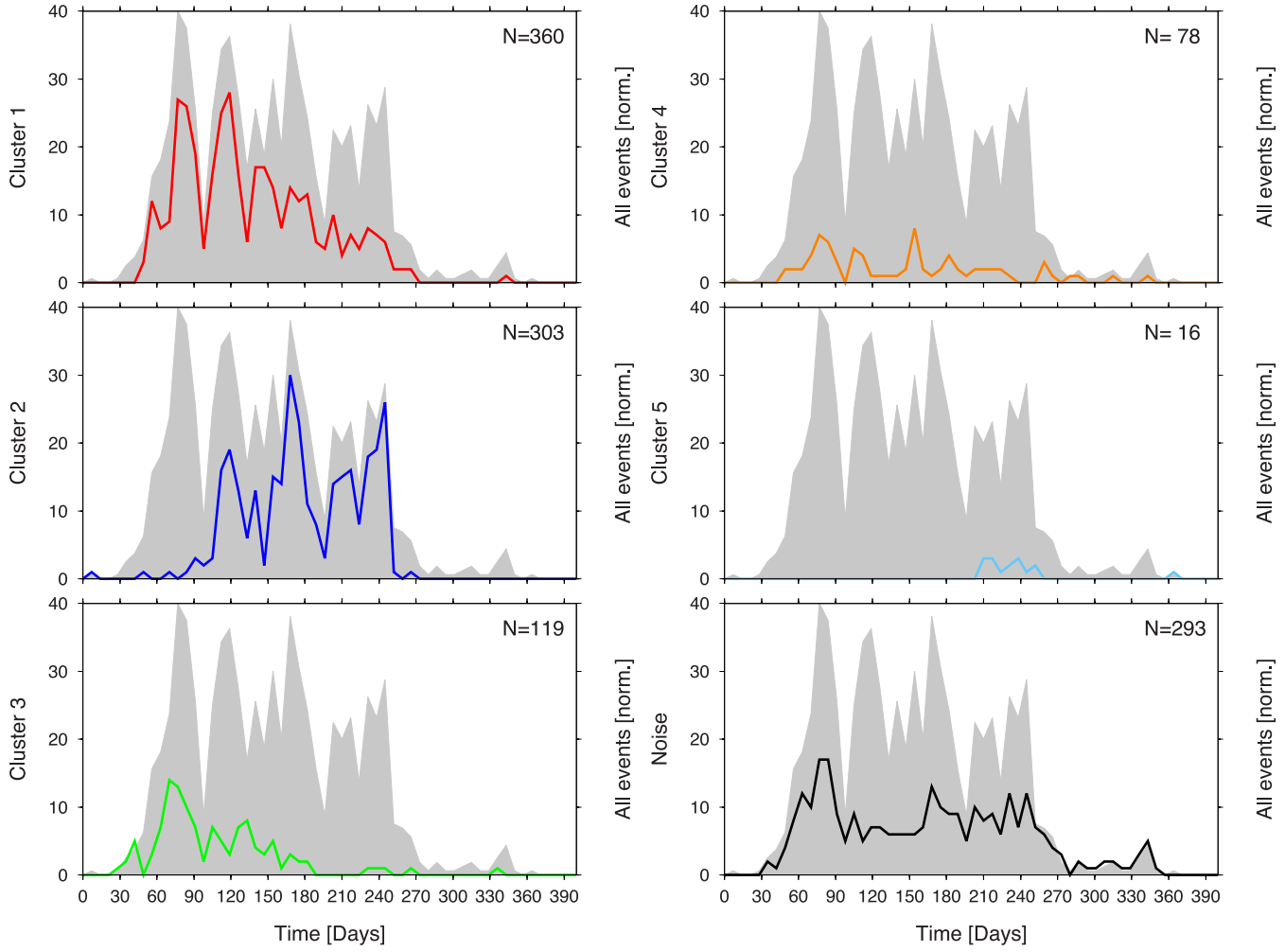

Figure 6. Temporal variation of the number of events from each cluster (colour curves according to the colour convention adopted in Fig. 4) and unclustered events (noise, black curve), with respect of the number of events with an available focal mechanism solution. Plots are shown for 400 d, starting on 2006 July 14, including the whole data set.

DISCUSSION

Moment tensor clustering showed to be a powerful tool for the automatic classification of catalogues of earthquake source parameters, the identification and characterization of source models families in different environments and regions, and the evaluation of temporal changes of the source models. The application to an induced seismicity catalogue at Hamm (Ruhr region, Germany) is suited to demonstrate the technique performance, as seismicity results strongly correlated to human activities, not only with respect to the spatial migration of epicentres with the mining advancement, but also for the characterization of the rupture processes, which is strongly linked to the mine geometry. The clustering technique, both applied to DC and full MT models is able to recognize the most important rupture patterns. The DC clustering approach identified the typical geometry of DC focal mechanisms, which resulted characterized by normal faulting mechanisms oriented parallel to the mining stope and panel sides. The MT clustering was unable to resolve the orientation of the DC terms, but could well detect the presence and sign of the non-DC component, which are in the current case associated to tensile components; this result is important towards the mining monitoring and hazard assessment. The choice of a specific metric (e.g. only considering full MT or DC component) will affect clustering results. Any future study should choose the most proper metric to answer the target scientific questions. For example, an analysis of fault plane orientations may be best discuss with the aid of a pure DC clustering approach, whereas the distribution of non-DC terms (e.g. in volcanic or mining environments) can only be judged using a full MT approach.

The method has a range of possible application for the analysis of broad seismicity catalogues in tectonic, volcanic or induced seismicity environments. Among its possible applications, we can foresee the investigation of repeated rupture processes in large data sets and microseismicity applications, the reconstruction of fault system geometries, the assessment of non-DC terms, and the identification of transient earthquake source and rupture anomalies. Depending on the goal of the source clustering, a preferred metric can be chosen. We have here proposed a variety of metrics, though other could be considered to answer specific seismological questions. For example, distances based only on the orientation of one fault plane angle, may be suited for the discussion of the orientation of specific faults or slab segments. Another important example may be given by distances definition on the base of the similarity of pressure and/or tension axis, which may be provide useful information towards stress inversion studies.

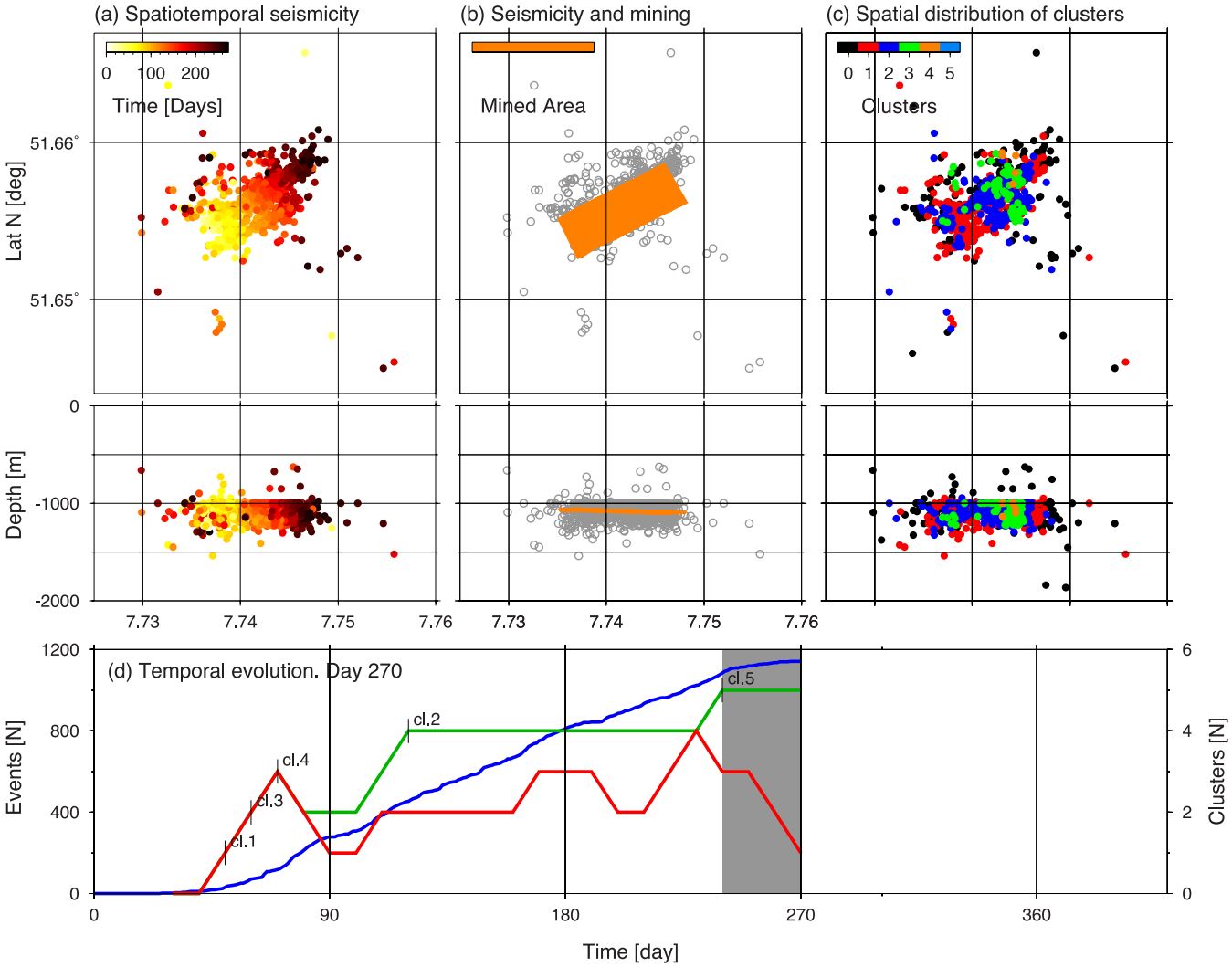

Figure 7. Snapshot (day 270 since 2006 July 14) of the seismicity monitoring framework, simulating the continuous monitoring applied to the Ruhr DC catalogue. Top plots illustrates the spatiotemporal evolution of seismicity as map and cross-section projection (top left, according to the given colour scale), the comparison of seismicity location and mined region (top centre, the mined region is denoted with an orange polygon), and the spatial distribution of different clusters (cluster colour scale according to convention used in Figs 4 and 6). The bottom panel illustrate the evolution of the number of detected clusters (thick red and green lines) and the cumulative number of event (thick blue line), as a function of time. The clustering is repeated every 10 d, after a first learning period of 30 d. The red curve is obtained considering only the seismicity recorded in the preceding 30 d (grey area), the green curve using all events until the running day. Thin black lines and cluster labels denote the appearance of clusters for the cumulative seismicity approach (green line).

Towards the adoption of the proposed technique for future studies, either dealing with natural or induced seismicity data sets, it is extremely important to remind that clustering results may be affected by the subjective choice of the clustering parameters. Limiting to the DBSCAN algorithm discussed in this work, a variable choice of $N_{\min}$ and ϵ parameters can strongly modify the number, size and average properties of the clusters. Fig. 8 attempts to summarize main effects of different parameter choices. In general, decreasing the parameter ϵ leads to the identification of more self-similar clusters and will tend to produce a larger number of small clusters. The number of cluster generally increases by reducing $N_{\min}$. The choice of clustering parameter should also account for the expected number of unclustered events. Increasing the size of the noise cluster is equivalent to a loss of information from the original catalogue, as the clustering result only can be used to assess the rupture process of a part of the studied seismicity. The number of unclustered events is typically correlated with the clustering parameters and can be reduced by increasing ϵ or by decreasing $N_{\min}$. Few anomalies can anyway be observed in Fig. 8, with the presence of darker belt-like regions of increased cluster numbers (Fig. 8a) and local scattering of the number of noise events (Fig. 8b). These effects are illustrated in Fig. 8(c): we repeated the clustering using a fixed ϵ (0.90) and four values of $N_{\min}$ (10, 15, 20, 25). In general, as expected, increasing $N_{\min}$ leads to smaller clusters, as only denser regions of the cluster are left. However, in the specific case one cluster (the red one) has an heterogeneous density with two denser regions, separated by a more sparse band. In such case, when increasing $N_{\min}$ from 15 to 20 the original red cluster is divided into two subclusters (red and cyan in the plot corresponding to $N_{\min}$ 20), temporally increasing from 4 to 5 the number of detected clusters. A further increment of $N_{\min}$, for example, to 25, results in the typical decrease in the clusters number, with the disappearance of the less populated clusters. The combination of such effects and the variable required cluster density, are similarly responsible for some sudden variations among the number of noise events of neighbouring ϵ–$N_{\min}$ configurations.

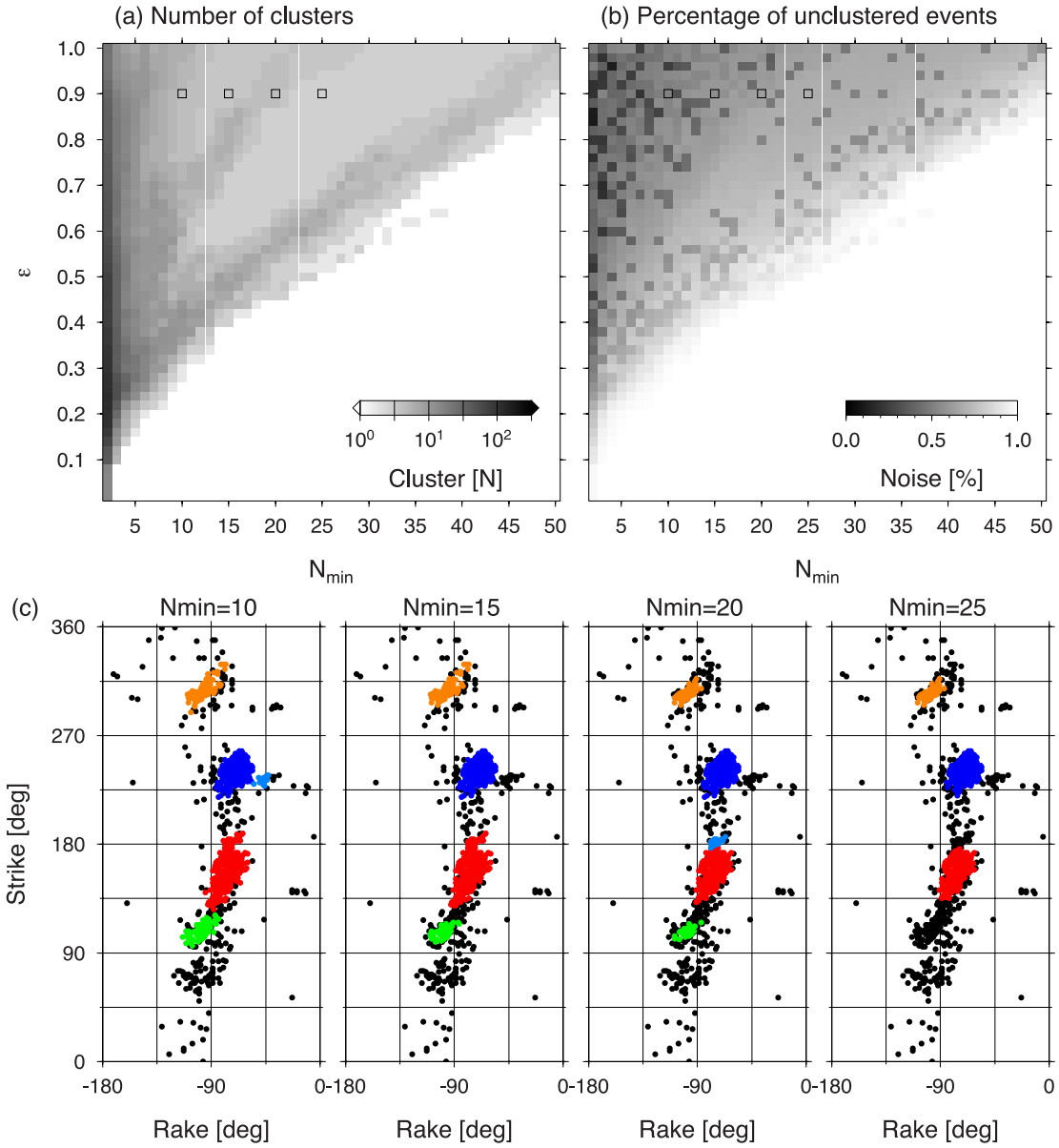

Figure 8. Performance of the DBSCAN algorithm with the pure DC catalogue from the Ruhr region (distance based on Kagan angle) when varying parameters $N_{\min}$ and epsilon. These plots illustrate how these parameters can change the number (and thus the average size) of clusters (top left-hand panel) and the number of non-classified (noise) focal mechanisms (top right-hand panel). Clustering results (bottom panels) are illustrated for the pure DC Ruhr data set using the Kagan angle distance, with epsilon 0.90 and four $N_{\min}$ values (the four used configurations are denoted by squares in the top left-hand plot). The analysis of the pure DC Ruhr data set has been performed with $N_{\min} = 10$ and $\epsilon = 0.90$.

A major potential of the clustering technique concerns its adoption within monitoring tools. The iterative clustering at different time can be used to detect the appearance, disappearance and evolution of clusters. In fact, if strong anomalous failure processes may be identified by the clustering approach, through the identification of a new cluster with anomalous average properties, it can also happen that the temporal stress perturbation only changes the average rupture mechanisms. For example, rupture may always take place along the same fault geometry (e.g. with strike and dip unchanged), and the effects of the temporal evolution of local stresses may only lead to a variation of the slip direction, along a more favourable configuration. Such effect may be seen through the appearance of a new cluster, if the rake change is considerable, but can also be detected for less dramatic changes by checking the time evolution of the average properties of the cluster. Cluster appearance (and disappearance) may also occur as a consequence of the clustering approach. A common case may be when one cluster becomes at a given time density-reachable from the second one, leading to a single, broader cluster. This can occur if the two clusters are close (similar) enough, when a sufficient number of outliers are present between them. A timely detection of anomalous ruptures is linked to the choice of clustering parameters. The occurrence of new fracturing processes can only be identified through the detection of a new cluster, which only takes place upon the inclusion of a sufficient number of events with the new source model in the catalogue. A quicker detection of new clusters can be achieved by reducing the parameter $N_{\min}$. However, this choice can also lead to false alarm, depending on the catalogue quality and the number of expected outlier solutions.

Finally, the possibility of combining clustering techniques based on different source parameters, such as focal mechanisms,

location, size, stress drop or seismicity rate, may be used to further investigate significant changes in the observed seismicity. However, such extension will need the definition of specific metrics, where different physical units have to be handled in a common distance definition.

CONCLUSIONS

A methodological approach and algorithm for moment tensor clustering and automated classification of earthquake point source models have been here presented and illustrated through application to synthetic and real data set. We could demonstrate the potential of the method for the automated detection and characterization of focal mechanisms clusters, which can be used to analyse large moment tensor catalogue. The availability of different metrics make possible to apply our method to different type of source representation.

We suggest the adoption of Kagan angle distance for pure DC catalogues, and weighted cosine distance for deviatoric and full moment tensor catalogues. Weights should be chosen on the base of moment tensor uncertainties, which are specific for different setups, and related to the adopted moment tensor inversion techniques, source-network geometries and velocity models. Other specific distance definition can be adopted, depending on the clustering application. On the other side, clustering parameters ($N_{\min}$ and ϵ) should be chosen carefully, and synthetic and real tests should be used to assess their effects on the clustering performance, which can be affected in terms of the number, size and self similarity of identified clusters. In particular the $N_{\min}$ value should be chosen with respect of the data set size (e.g. increasing with the size of the data set) and the desired resolution among close clusters: these can only be discriminated if the intercluster regions are judged by the algorithm as sparsely populated. The ϵ parameter should be chosen according to the desired degree of similarity within each cluster (small ϵ will lead to homogeneous clusters composed of very similar focal mechanisms) and upon the adopted metrics.

The application to an induced seismicity catalogue, following the exploitation of a coal mine panel in the Ruhr region, Germany, lead to the identification of main seismic source families. Based on the DC catalogue, we identified five families of events, with normal faulting of different orientations. Striking correspond to the orientation of the panel sides and stope. Full moment tensor clustering identified two main event families, based on the presence of positive and negative tensile components. The analysis of the temporal distribution of clusters indicate that during the first part of the longwall mining, ruptures are dominated by NNW–SSE strike faulting, parallel to the mining stope. During the second part of the exploitation, mostly from day 150, most induced earthquakes were instead characterized by a WSW–ENE striking, parallel to the panel sides.

The method is potentially of interest for monitoring of natural and induced seismicity, in active tectonic, volcanic, geothermal and mining environments. The adoption of the clustering tool for monitoring purposes can be used to identify the appearance or disappearance of rupture clusters, and significant variation of fracturing processes or local stress, thus providing important information for the temporal reassessment of seismic hazard.

ACKNOWLEDGEMENTS

The authors wish to thank Prof Dr Jan Šílený and an anonymous reviewer for comments and suggestions, and Prof Dr Frank Krüger for valuable discussions. The used mining seismicity moment tensor catalogue (Şen *et al*. 2013) was generated thanks to the monitoring and processing work carried out by the Ruhr University Bochum, for which we particularly acknowledge Prof Dr Thomas Meier and Ms Monika Bischoff. Figures and DC focal mechanisms have been plotted with GMT (Wessel & Smith 1998). Moment tensor decomposition and plotting is carried out using the Mopad tool (Krieger & Heimann 2012), which is routinely used by the software MTD. This work has been funded by the German BMBF 'Geotechnologien' project MINE (Grant of project BMBF03G0737).

REFERENCES

Aki, K. & Richards, P.G., 1980. *Quantitative Seismology, Theory and Methods*, Freeman & Co.

Becker, D., Cailleau, B., Dahm, T., Shapiro, S. & Kaiser, D., 2010. Stress triggering and stress memory observed from acoustic emission records in a salt mine, *Geophys. J. Int.,* **182,** 933–948.

Bernardi, F., Braunmiller, J., Kradolfer, U. & Giardini, D., 2004. Automatic regional moment tensor inversion in the European-Mediterranean region, *Geophys. J. Int.,* **157,** 703–716.

Bischoff, M., Cete, A., Fritschen, R. & Meier, T., 2010. Coal mining induced seismicity in the Ruhr area, Germany, *Pure appl. Geophys.,* **167,** 63–75.

Boyd, O.S., Dreger, D.S., Hellweg, M., Lombard, P.N., Ford, S.R., Taira, T., Taggart, J. & Weldon, T.J., 2011. Full moment tensor analysis using first motion data at the geysers geothermal field, *Am. Geophys. Un.,* Fall Meeting 2011, abstract #S33A-2301.

Buforn, E., Pro, C., Cesca, S., Udías, A. & del Fresno, C., 2011. The 2010 Granada (Spain) earthquake, *Bull. seism. Soc. Am.,* **101**(5), 2418–2430.

Bukchin, B., Clevede, E. & Mostinskiy, A., 2010. Uncertainty of moment tensor determination from surface wave analysis for shallow earthquakes, *J. Seismol.,* **14,** 601–614.

Cattaneo, M., Augliera, P., Spallarossa, D. & Lanza, V., 1999. A waveform similarity approach to investigate seismicity patterns, *Nat. Hazard,* **19,** 123–138.

Cesca, S. & Dahm, T., 2008. A frequency domain inversion code to retrieve time-dependent parameters of long period volcanic sources, *Comput. Geosci.,* **34**(3), 235–246.

Cesca, S., Braun, T., Tessmer, E. & Dahm, T., 2007. Modelling of the April 5, 2003 Stròmboli (Italy) paroxysmal eruption from the inversion of broadband seismic data, *Earth planet. Sci. Lett.,* **261**(1–2), 164–178.

Cesca, S., Battaglia, J., Dahm, T., Tessmer, E., Heimann, S. & Okubo, P., 2008. Effects of topography and crustal heterogeneitiies on the source estimation of LP events at Kilauea volcano, *Geophys. J. Int.,* **172**(3), 1219–1236.

Cesca, S., Rohr, A. & Dahm, T., 2013. Discrimination of induced seismicity by full moment tensor inversion and decomposition, *J. Seismol.,* **17,** 147–163.

Chouet, B. *et al.*, 2003. Source mechanisms of explosions at Stromboli Volcano, Italy, determined from moment-tensor inversions of very-long-period data, *J. geophys. Res.,* **108,** 2019.

Davi, R., O'Brien, G.S., Lokmer, I., Bean, C.J., Lesage, P. & Mora, M., 2010. Moment tensor inversion of explosive long period events recorded on Arenal Volcano, Costa Rica, constrained by synthetic tests, *J. Volc. Geotherm. Res.,* **194**(4), 189–200.

Du, J. & Warpinski, N.R., 2011. Uncertainty in FPSs from moment-tensor inversion, *Geophysics,* **76**(6), WC65–WC75.

Dziewonski, A.M., Chou, T.A. & Woodhouse, J.H., 1981. Determination of earthquake source parameters from waveform data for studies of global and regional seismicity, *J. Geophys. Res.,* **86,** 2825–2852.

Ekström, G., Nettles, M. & Dziewonski, A.M., 2012. The global CMT project 2004–2010: centroid-moment tensors for 13,017 earthquakes, *Phys. Earth Planet. Inter.,* **200–201,** 1–9.

Ester, M., Kriegel, H.-P., Sander, J. & Xu, X., 1996. A density-based algorithm for discovering clusters in large spatial databases with noise, in *Proceedings of the Second International Conference on Knowledge*

Discovery and Data Mining, pp. 226–231, eds Simoudis, E., Han, J. & Fayyad, U.M., AAAI Press.

Feignier, B. & Young, R.P., 1992. Moment tensor inversion of induced microseismic events: evidence of non-shear failures in the -4<M<-2 moment magnitude range, *Geophys. Res. Lett.,* **19**(14), 1503–1506.

Fletcher, J.B. & McGarr, A., 2005. Moment tensor inversion of ground motion from mining induced earthquakes, Trail mountain, Utah, *Bull. seism. Soc. Am.,* **5**(1), 48–57.

Foulger, G.R. & Julian, B.R., 1993. Non-double couple earthquakes at the Hengill-Grensdalur volcanic complex, Iceland: are they the artifacts of crustal heterogeneity? *Bull. seism. Soc. Am.,* **83,** 38–52.

Frolich, C., 1995. Characteristic of well-determined non-double-couple earthquakes in the Harvard CMT catalog, *Phys. Earth planet. Inter.,* **91,** doi:10.1016/0031-9201(95)03031-Q.

Giardini, D., Boschi, E. & Palombo, B., 1993. Moment tensor inversion from Mednet data (2) Regional earthquakes of the Mediterranean, *Geophys. Res. Lett.,* **20,** 273–276.

Grigoli, F., Cesca, S., Vassallo, M. & Dahm, T., 2013. Automated seismic event location by traveltime stacking: an application to mining induced seismicity, *Seismol. Res. Lett.,* **84**(4), 666–677.

Hainzl, S., Zöller, G. & Kurths, J., 2000. Self-organization of spatio-temporal o f earthquake clusters, *Nonlin. Process. Geophys.,* **7,** 21–29.

Henry, C., Woodhouse, J.H. & Das, S., 2002. Stability of earthquake moment tensor inversions: effect of the double-couple constraints, *Tectonophysics,* **356,** 115–124.

Hudson, J.A., Pearce, R.G. & Rogers, R.M., 1989. Source Type plot for inversion of the moment tensor, *J. geophys. Res.,* **94,** 765–774.

Jost, M.L. & Hermann, R.B., 1989. A students guide to and review of moment tensors, *Seismol. Res. Lett.,* **60,** 37–57.

Julià, J., Nyblade, A.A., Durrheim, R., Linzer, L., Gok, R., Dirks, P. & Walter, W., 2009. Source mechanisms of mine-related seismicity, Savuka mine, South Africa, *Bull. seism. Soc. Am.,* **99,** 2801–2814.

Julian, B.R., Miller, A.D. & Foulger, G.R., 1998. Non-double-couple earthquakes, 1, *Theor. Rev. Geophys.,* **36**(4), 525–549.

Kagan, Y.Y., 1991. 3-D rotation of double-couple earthquake sources, *Geophys. J. Int.,* **106,** 709–716.

Kagan, Y.Y., 1992. Correlation of earthquake focal mechanisms, *Geophys. J. Int.,* **110,** 305–320.

Kagan, Y.Y. & Jackson, D.D., 1991. Long-term earthquake clustering, *Geophys. J. Int.,* **104,** 117–133.

Kagan, Y.Y. & Knopoff, L., 1976. Statistical search for non-random features of the seismicity of strong earthquakes, *Phys. Earth planet. Int.,* **12,** 291–318.

Kaneshima, S. *et al.*, 1996. Mechanism of phreatic eruptions at Aso Volcano inferred from near-field broadband seismic observations, *Science,* **273,** 642–645.

Knopoff, L. & Randall, M.J., 1970 The compensated linear vector dipole: a possible mechanism for deep earthquakes, *J. geophys. Res.,* **75,** 4957–4963.

Konstantaras, A.J., Katsifarakis, E., Maravelaiks, E., Skounakis, E., Kokkinos, E. & Karapidakis, E., 2012. Intelligent spatial-clustering of seismicity in the vicinity of the Hellenic seismic arc, *Earth Sci. Res.,* **1,** doi:10.5539/esr.v1n2p1.

Kravanja, S., Batini, F., Fiordelisi, A. & Panza, G.F., 1999. Full moment tensor retrieval waveform inversion in the Larderello geothermal area, *Pure appl. Geophys.,* **157,** 1379–1392.

Krieger, L. & Heimann, S., 2012. MoPaD—moment tensor plotting and decomposition: a tool for graphical and numerical analysis of seismic moment tensors, *Seismol. Res. Lett.,* **83,** 589–595.

Kuge, K. & Kawakatsu, H., 1990. Analysis of a deep "non double couple" earthquake using very broadband data, *Geophys. Res. Lett.,* **17,** 227–230.

Kuge, K. & Kawakatsu, H., 1992. Deep and intermediate-depth non-double-couple earthquakes: interpretation of moment tensor inversions using very broadband seismic waves, *Geophys. J. Int.,* **111,** 589–606.

Kuge, K. & Kawakatsu, H., 1993. Significance of non-double couple components of deep and intermediate-depth earthquakes: implication from moment tensor inversions of various long-period seismic waves, *Phys. Earth planet. Inter.,* **75,** 243–266.

Kühn, D. & Vavryčuk, V., 2013. Determination of full moment tensors in a very heterogeneous mining environment, *Tectonophysics,* **589,** 33–43.

Legrand, D., Kaneshima, S. & Kawakatsu, H., 2000. Moment tensor analysis of near-field broadband waveforms observed at Aso Volcano, Japan, *J. Volc. Geotherm. Res.,* **101,** 155–169.

Lippiello, E., Marzocchi, W., de Arcangelis, L. & Godano, C., 2012. Spatial organization of foreshocks as a tool to forecast large earthquakes, *Scient. Rep.,* **2,** doi:10.1038/srep00846.

Lokmer, I., Bean, C.J., Saccorotti, G. & Patanè, D., 2007. Moment-tensor inversion of LP events recorded on Etna in 2004 using constraints obtained from wave simulation tests, *Geophys. Res. Lett.,* **34,** L22316, doi:10.1029/2007GL031902.

Maurer, H. & Deichmann, N., 1995. Microearthquake cluster detection based on waveform similarities, with an application to the western Swiss Alps, *Geophys. J. Int.,* **123,** 588–600.

McGarr, A., 1992. An implosive component in the seismic moment tensor of a mining-Induced tremor, *Geophys. Res. Lett.,* **19,** 1579–1582.

McGarr, A., 1992. Moment tensors of ten witwatersrand mine tremors, *Pure appl. Geophys.,* **139,** 781–800.

Ouillon, G. & Sournette, D., 2011. Segmentation of fault networks determined from spatial clustering of earthquakes, *J. geophys. Res.,* **116,** B2, doi:10.1029/2010JB007752.

Panza, G.F. & Saraò, A., 2000. Monitoring volcanic and geothermal areas full seismic moment tensor inversion: are non-double-couple components always artefacts of modelling? *Geophys. J. Int.,* **143,** 353–364.

Panza, G.F., Sileny, J., Campus, P., Nicolich, R. & Ranieri, G., 1993. Point source moment tensor retrieval in volcanic, geothermal and orogenic areas by complete waveform inversion, *Int. J. appl. Geophys.,* **30,** 98–118.

Pedregosa, F. *et al.*, 2011. Scikit-learn: machine learning in Pyhton, *J. Mach. Learn. Res.,* **12,** 2825–2830.

Pondrelli, S., Morelli, A., Ekström, G., Mazza, S., Boschi, E. & Dziewonski, A.M., 2002. European-Mediterranean regional centroid-moment tensors: 1997–2000, *Phys. Earth planet. Int.,* **130,** 71–101.

Ritsema, J. & Lay, T., 1993. Rapid source mechanism determination of large (Mw > 4.5) in western United States, *Geophys. Res. Lett.,* **20,** 1611–1614.

Ross, A., Foulger, G.R. & Julian, B.R., 1999. Source processes of industrially-induced earthquakes at the Geysers geothermal area, California, *Geophysics,* **64**(6), 1877–1889.

Saraò, A., Panza, G.F., Privitera, E. & Cocina, O., 2001. Non-double couple mechanisms in the seismicity preceding 1991–93 Etna volcano eruption, *Geophys. J. Int.,* **145**(2), 319–335.

Şen, A.T., Cesca, S., Bischoff, M., Meier, T. & Dahm, T., 2013. Automated full moment tensor inversion of coal mining induced seismicity, *Geophys. J. Int.,* **195,** 1267–1281.

Sornette, D. & Werner, M.J., 2005. Apparent clustering and apparent background earthquakes biased by undetected seismicity, *J. geophys. Res.,* **110,** B9, doi:10.1029/2005JB003621.

Stich, D., Ammon, C.J. & Morales, J., 2003. Moment tensor solutions for small and moderate earthquakes in the Ibero-Maghreb region, *J. geophys. Res.,* **108**(B3), 2148, doi:10.1029/2002JB002057.

Tape, W. & Tape, C., 2012. Angle between principal axis triples, *Geophys. J. Int.,* **191,** 813–831.

Trifu, C.-I., Angus, D. & Shumila, V., 2000. A fast evaluation of the seismic moment tensor for induced seismicity, *Bull. seism. Soc. Am.,* **90,** 1521–1527.

Vavryčuk, V. & Kühn, D., 2012. Moment tensor inversion of waveforms: a two-step time-frequency approach, *Geophys. J. Int.,* **190,** 1761–1776.

Wehling-Benatelli, S., Becker, D., Bischoff, M., Friederich, W. & Meier, T., 2013. Indications for different types of brittle failure due to active coal mining using waveform similarities of induced seismic events, *Solid Earth Discuss.,* **5**(1), 655–698.

Wessel, P. & Smith, W.H.F., 1998. New, improved version of generic mapping tools released, *EOS, Trans. Am. geophys. Un.,* **79,** 579–579.

Willemann, R.J., 1993. Cluster analysis of seismic moment tensor orientations, *Geophys. J. Int.,* **115,** 617–634.